Cancer Cell, Volume *34*

Supplemental Information

Synthetic Lethal and Convergent Biological Effects of Cancer-Associated Spliceosomal Gene Mutations

Stanley Chun-Wei Lee, Khrystyna North, Eunhee Kim, Eunjung Jang, Esther Obeng, Sydney X. Lu, Bo Liu, Daichi Inoue, Akihide Yoshimi, Michelle Ki, Mirae Yeo, Xiao Jing Zhang, Min Kyung Kim, Hana Cho, Young Rock Chung, Justin Taylor, Benjamin H. Durham, Young Joon Kim, Alessandro Pastore, Sebastien Monette, James Palacino, Michael Seiler, Silvia Buonamici, Peter G. Smith, Benjamin L. Ebert, Robert K. Bradley, and Omar Abdel-Wahab

Figure S1

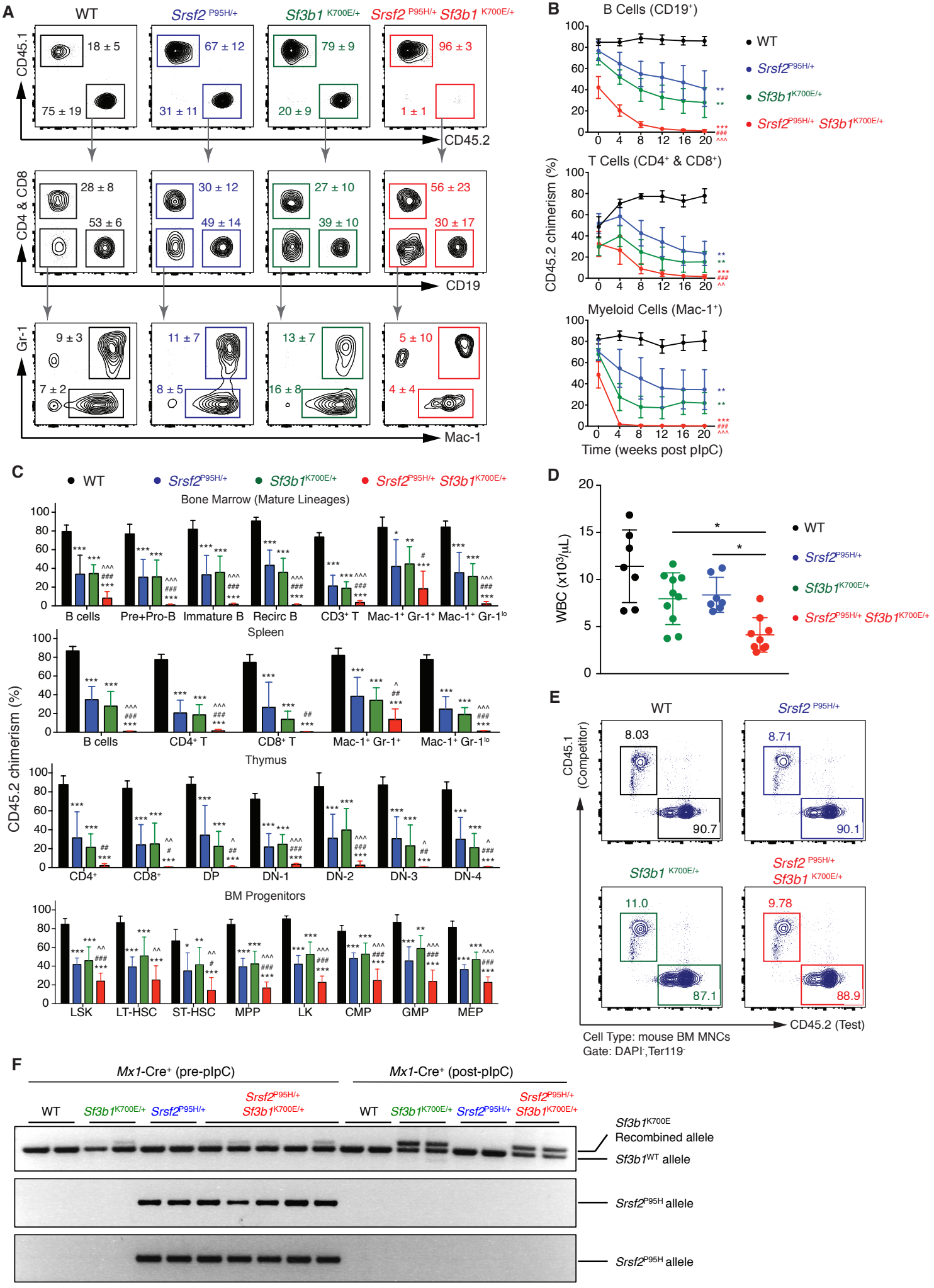
A
WT
Srsf2 P95H/+
Sf3b1 K700E/+
Srsf2 P95H/+ Sf3b1 K700E/+
CD45.1
CD45.2
18 ± 5
75 ± 19
67 ± 12
31 ± 11
79 ± 9
20 ± 9
96 ± 3
1 ± 1
CD4 & CD8
28 ± 8
53 ± 6
30 ± 12
49 ± 14
27 ± 10
39 ± 10
56 ± 23
30 ± 17
CD19
Gr-1
9 ± 3
7 ± 2
11 ± 7
8 ± 5
13 ± 7
16 ± 8
5 ± 10
4 ± 4
Mac-1
B
B Cells (CD19+)
T Cells (CD4+ & CD8+)
Myeloid Cells (Mac-1+)
CD45.2 chimerism (%)
Time (weeks post pIpC)
C
Bone Marrow (Mature Lineages)
B cells
Pre+Pro-B
Immature B
Recirc B
CD3+ T
Mac-1+ Gr-1+
Mac-1+ Gr-1lo
Spleen
CD4+ T
CD8+ T
Thymus
CD4+
CD8+
DP
DN-1
DN-2
DN-3
DN-4
BM Progenitors
LSK
LT-HSC
ST-HSC
MPP
LK
CMP
GMP
MEP
D
WBC (x10³/μL)
E
CD45.1 (Competitor)
8.03
90.7
8.71
90.1
11.0
87.1
9.78
88.9
CD45.2 (Test)
Cell Type: mouse BM MNCs
Gate: DAPI-,Ter119-
F
Mx1-Cre+ (pre-pIpC)
Mx1-Cre+ (post-pIpC)
Sf3b1K700E Recombined allele
Sf3b1WT allele
Srsf2P95H allele
Srsf2P95H allele

Figure S1

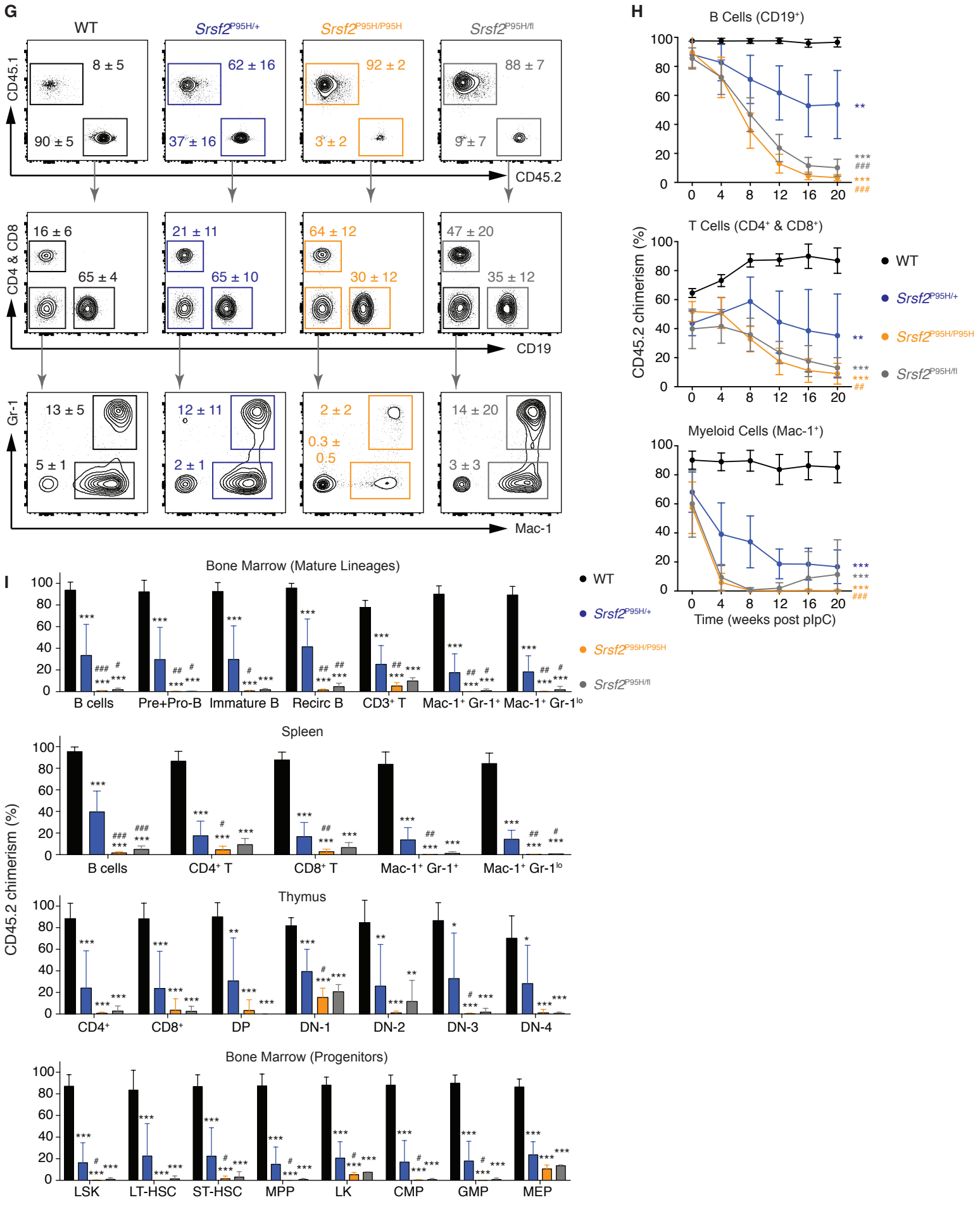
G
WT
Srsf2P95H/+
Srsf2P95H/P95H
Srsf2P95H/fl
CD45.1
CD45.2
8 ± 5
90 ± 5
62 ± 16
37 ± 16
92 ± 2
3 ± 2
88 ± 7
9 ± 7
CD4 & CD8
CD19
16 ± 6
65 ± 4
21 ± 11
65 ± 10
64 ± 12
30 ± 12
47 ± 20
35 ± 12
Gr-1
Mac-1
13 ± 5
5 ± 1
12 ± 11
2 ± 1
2 ± 2
0.3 ± 0.5
14 ± 20
3 ± 3
H
B Cells (CD19+)
T Cells (CD4+ & CD8+)
Myeloid Cells (Mac-1+)
CD45.2 chimerism (%)
Time (weeks post pIpC)
WT
Srsf2P95H/+
Srsf2P95H/P95H
Srsf2P95H/fl
I
Bone Marrow (Mature Lineages)
B cells
Pre+Pro-B
Immature B
Recirc B
CD3+ T
Mac-1+ Gr-1+
Mac-1+ Gr-1lo
Spleen
CD4+ T
CD8+ T
Thymus
CD4+
CD8+
DP
DN-1
DN-2
DN-3
DN-4
Bone Marrow (Progenitors)
LSK
LT-HSC
ST-HSC
MPP
LK
CMP
GMP
MEP

Figure S1 (Related to Figure 1). Severe self-renewal disadvantage of hematopoietic stem cells from *Srsf2*$^{P95H/+}$ *Sf3b1*$^{K700E/+}$ double-mutant and *Srsf2*$^{P95H/P95H}$ homozygous mutant mice. (A) Representative FACS plots of CD45.2 (donor-derived) cells of both lymphoid and myeloid lineages in the peripheral blood of CD45.1 recipient mice reconstituted with bone marrow (BM) mononuclear cells (MNCs) from *Mx1*-Cre^{+} WT, *Mx1*-Cre^{+} *Srsf2*$^{P95H/+}$, *Mx1*-Cre^{+} *Sf3b1*$^{K700E/+}$ and *Mx1*-Cre^{+} *Srsf2*$^{P95H/+}$ *Sf3b1*$^{K700E/+}$ mice 20 weeks post pIpC administration. **(B)** CD45.2 (donor-derived) chimerism in the B, T or myeloid lineages in peripheral blood (PB) of CD45.1 recipient mice (n=10 mice per genotype) in competitive BM transplantation (BMT). **(C)** Analysis of CD45.2 chimerism in the various cellular lineages in the bone marrow, spleen and thymus 20 weeks post pIpC administration in CD45.1 recipient mice. **(D)** White blood cell (WBC) count of *Mx1*-Cre^{+} WT, *Mx1*-Cre^{+} *Srsf2*$^{P95H/+}$, *Mx1*-Cre^{+} *Sf3b1*$^{K700E/+}$ and *Mx1*-Cre^{+} *Srsf2*$^{P95H/+}$ *Sf3b1*$^{K700E/+}$ mice 52 weeks post pIpC administration. **(E)** Representative FACS plots of BM MNC samples prior to noncompetitive BMT. **(F)** Representative genotyping PCR gel of PB MNCs of *Mx1*-Cre^{+} WT, *Mx1*-Cre^{+} *Srsf2*$^{P95H/+}$, *Mx1*-Cre^{+} *Sf3b1*$^{K700E/+}$ and *Mx1*-Cre^{+} *Srsf2*$^{P95H/+}$ *Sf3b1*$^{K700E/+}$ mice pre- and post-pIpC administration. Two separate PCR strategies were used for to detect *Srsf2*^{P95H} recombination. Successful allele recombination is shown by the absence of a PCR product. **(G)** Representative FACS plots of CD45.2 (donor-derived) cells of both lymphoid and myeloid lineages in the peripheral blood of CD45.1 recipient mice reconstituted with bone marrow (BM) mononuclear cells (MNCs) from *Mx1*-Cre^{+} WT, *Mx1*-Cre^{+} *Srsf2*$^{P95H/+}$, *Mx1*-Cre^{+} *Srsf2*$^{P95H/P95H}$ and *Mx1*-Cre^{+} *Srsf2*$^{P95H/fl}$ mice 20 weeks post pIpC administration. **(H)** Percentage of CD45.2 (donor-derived) chimerism in the B, T or myeloid lineages in peripheral blood of CD45.1 recipient mice (n=5-10 mice per genotype) in competitive BMT. **(I)** Analysis of CD45.2 chimerism in the various cellular lineages in the bone marrow, spleen and thymus 20 weeks post pIpC administration in CD45.1 recipient mice. Error bars represent mean±standard deviation. Analysis of variance followed by Tukey's post-hoc test was used to compare differences between groups. *p<0.05, **p<0.01 and ***p<0.001 versus *Mx1*-Cre^{+} WT mice; ^p<0.05, ^^p<0.01 and ^^^p<0.001 versus *Mx1*-Cre^{+} *Sf3b1*$^{K700E/+}$ mice; $^{\#}$p<0.05, $^{\#\#}$p<0.01 and $^{\#\#\#}$p<0.001 versus *Mx1*-Cre^{+} *Srsf2*$^{P95H/+}$ mice.

Figure S2

A

E14.5 embryos (n=139)	*Vav*-Cre$^+$	*Vav*-Cre$^-$
WT	14.3% (20/139)	10.8% (15/139)
Srsf2$^{P95H/+}$	13.7% (19/139)	13.7% (19/139)
Sf3b1$^{K700E/+}$	10.8% (15/139)	12.2% (17/139)
Srsf2$^{P95H/+}$ *Sf3b1*$^{K700E/+}$	10.8% (15/139)	13.7% (19/139)

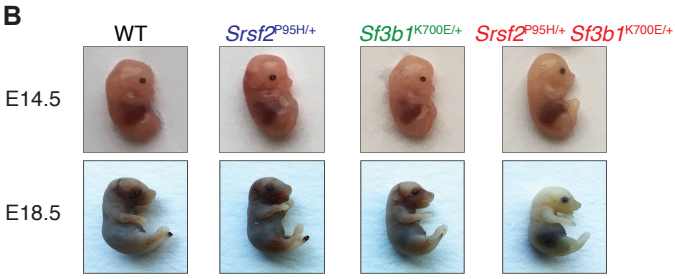

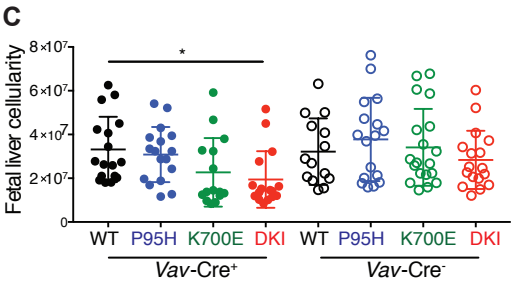

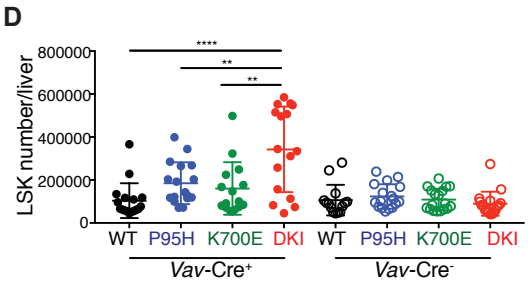

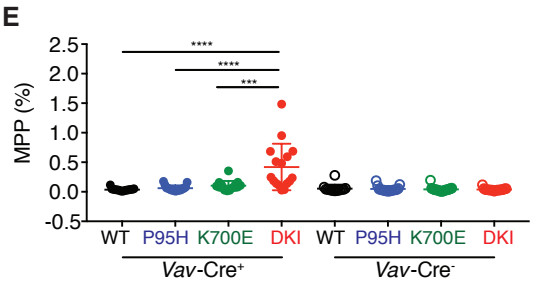

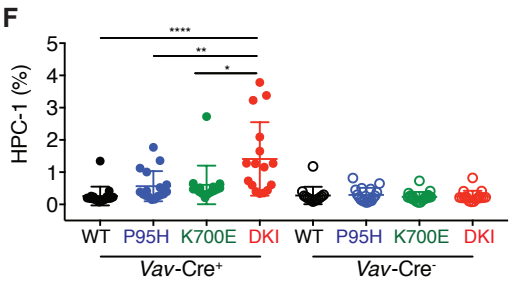

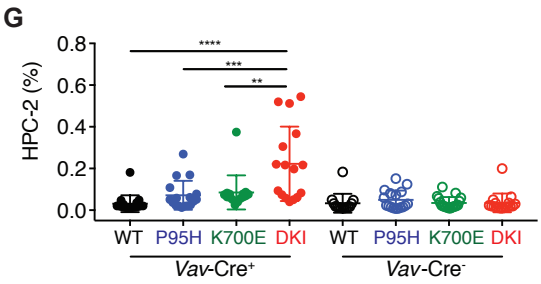

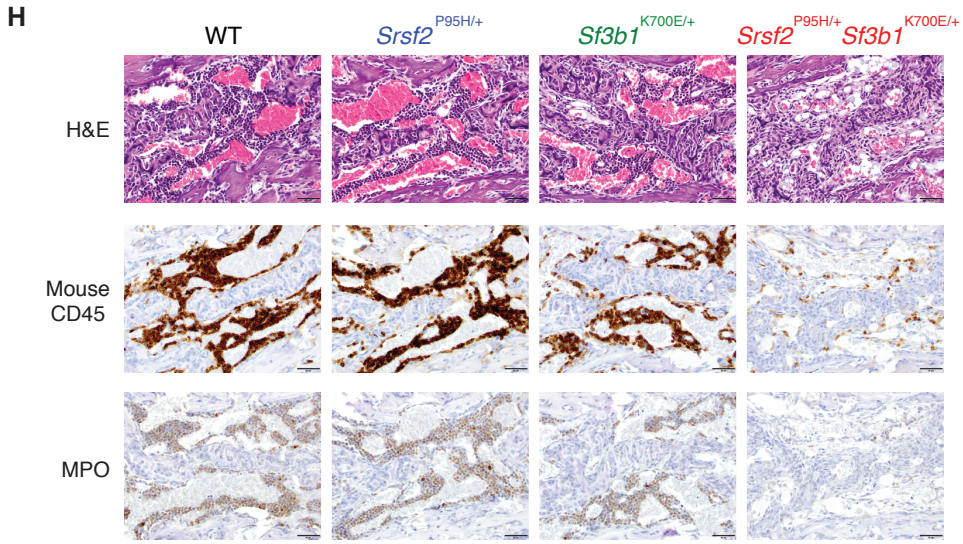

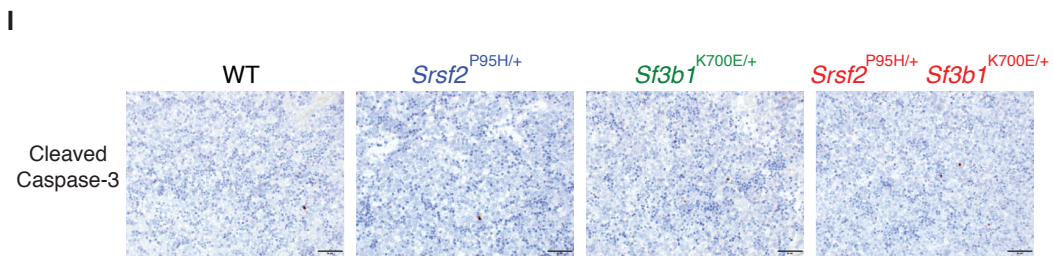

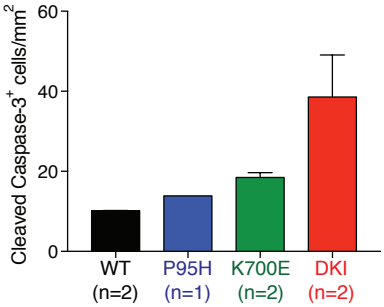

Figure S2 (Related to Figure 2). Co-expression of *Srsf2* and *Sf3b1* mutations results in death before birth in *Vav*-Cre^{+} *Srsf2*$^{P95H/+}$ *Sf3b1*$^{K700E/+}$ mice. (A) Number of embryos detected at embryonic day 14.5 (E14.5) per genotype from crossing *Sf3b1*$^{K700E/+}$ x *Vav*-Cre^{+} *Srsf2*$^{P95H/+}$ or *Srsf2*$^{P95H/+}$ x *Vav*-Cre^{+} *Sf3b1*$^{K700E/+}$ mice. **(B)** Photographs of representative fetuses with each genotype at E14.5 and E18.5. **(C)** Number of viable fetal liver mononuclear cells (MNCs) and **(D)** LSK (Lin^{-} Sca-1^{+} c-Kit^{+}) cells from E14.5 embryos from (A). Frequency of **(E)** MPP (LSK CD48^{-} CD150^{-}), **(F)** HPC-1 (LSK CD48^{+} CD150^{-}), and **(G)** HPC-2 (LSK CD48^{+} CD150^{+}) cells amongst fetal liver MNCs at E14.5. **(H)** Photomicrographs of hematoxylin and eosin (H&E), anti-CD45, and anti-myeloperoxidase (MPO) immunohistochemical stains of E18.5 marrow cavity cells of the mice in (B). **(I)** Photomicrographs of cleaved caspase-3 immunohistochemical stains of E18.5 fetal liver cells of the mice in (B) with quantitation on right. Error bars represent mean±standard deviation. Analysis of variance followed by Tukey's post-hoc test was used to compare differences between groups. *p<0.05, **p<0.01, ***p<0.001, and ****p<0.0001.

Figure S3

A

	Genotypes Compared	Expected		Observed		p value
		Convergent	Total	Convergent	Total	
A	*Sf3b1*$^{K700E/+}$ *Srsf2*$^{P95H/+}$ *Sf3b1*$^{K700E/+}$	186	431	197	429	0.23
	Srsf2$^{P95H/+}$ *Srsf2*$^{P95H/+}$ *Sf3b1*$^{K700E/+}$	143	232	135	236	0.81
B	*Sf3b1*$^{K700E/+}$ *Srsf2*$^{P95H/+}$ *Sf3b1*$^{K700E/+}$	108	248	90	241	0.90
	Srsf2$^{P95H/+}$ *Srsf2*$^{P95H/+}$ *Sf3b1*$^{K700E/+}$	161	385	161	378	0.44
C	*Sf3b1*$^{K700E/+}$ *Srsf2*$^{P95H/+}$ *Sf3b1*$^{K700E/+}$	121	239	87	233	0.99
	Srsf2$^{P95H/+}$ *Srsf2*$^{P95H/+}$ *Sf3b1*$^{K700E/+}$	108	198	99	198	0.79

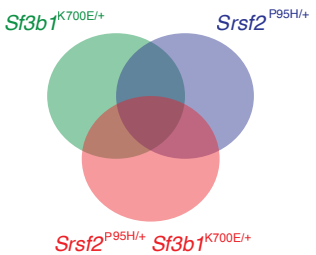

B

	Expected		Observed		p value
	Dysregulated	Expressed Coding	Dysregulated	Expressed Coding	
A	217	11031	275	10943	3.6×10^{-3}
B	187	11007	563	10759	2.2×10^{-16}
C	143	11026	261	10793	5.5×10^{-10}

C

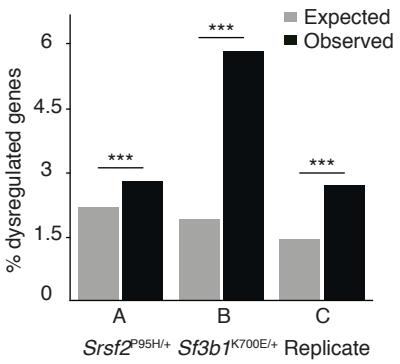

Figure S3 (Related to Figure 3). *Srsf2* and *Sf3b1* mutations have distinct and independent effects on gene dysregulation. (A) Table illustrating the numbers of expected versus observed coding genes exhibiting dysregulated expression that were shared between the illustrated comparisons between genotypes ("A", "B", and "C" refer to replicates of RNA-seq). The set of expected coding genes exhibiting dysregulation was defined assuming that the *Sf3b1* and *Srsf2* mutations were independent, such that the double-mutant gene expression program was simply the mean of the two single-mutant gene expression programs. "Convergent" is defined as the number of differentially expressed genes shared by the genotypes compared. "Total" is defined as the number of differentially expressed genes in the first genotype listed per category. p values were computed using the one-sided binomial proportion test. **(B)** Table illustrating the numbers of expected versus observed coding genes that were dysregulated in double-mutant cells relative to wild-type cells. The set of expected coding genes exhibiting dysregulation was defined as in (A). **(C)** Bar plots showing percentage (%) of expected versus observed coding genes exhibiting dysregulated expression in each replicate of *Mx1*-Cre^{+} *Srsf2*$^{P95H/+}$ *Sf3b1*$^{K700E/+}$ cells relative to *Mx1*-Cre^{+} WT cells. ***p<0.0001.

Figure S4

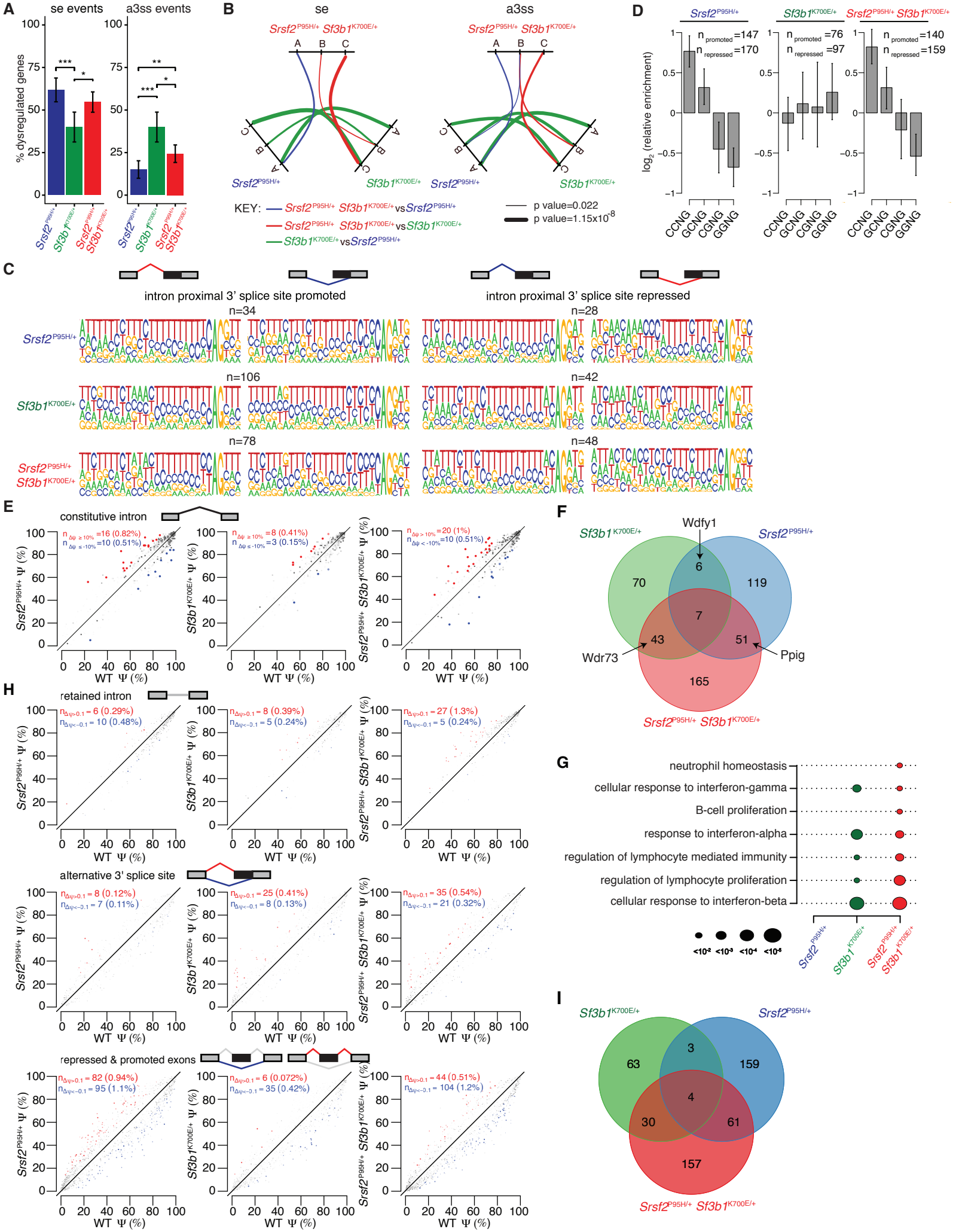
A
se events
a3ss events
% dysregulated genes
B
se
a3ss
KEY:
p value=0.022
p value=1.15x10-8
C
intron proximal 3' splice site promoted
intron proximal 3' splice site repressed
n=34
n=28
n=106
n=42
n=78
n=48
D
log2 (relative enrichment)
CCNG
GCNG
CGNG
GGNG
E
constitutive intron
WT Ψ (%)
F
Wdfy1
70
6
119
7
43
51
Wdr73
Ppig
165
G
neutrophil homeostasis
cellular response to interferon-gamma
B-cell proliferation
response to interferon-alpha
regulation of lymphocyte mediated immunity
regulation of lymphocyte proliferation
cellular response to interferon-beta
H
retained intron
alternative 3' splice site
repressed & promoted exons
I
63
3
159
4
30
61
157

Figure S4 (Related to Figure 4). *Srsf2* and *Sf3b1* mutations have distinct and independent effects on RNA splicing. (A) Bar plot illustrating the percentage of dysregulated splicing events that corresponded to cassette exon events (se; left) or competing 3' splice site events (a3ss; right) for each illustrated genotype relative to wild-type cells. P values were computed using a two sided binomial proportion test where **p<0.01 and ***p<0.001. **(B)** Diagram illustrating whether there was a statistically significant difference in the fraction of dysregulated splicing events corresponding to cassette exon events (se; left) or competing 3' splice site events (a3ss; right). P values were computed using the binomial proportion test and are represented by the thickness of the lines. **(C)** Sequence logos associated with competing 3' splice sites that are differentially spliced in *Mx1*-Cre^{+} *Srsf2*$^{P95H/+}$, *Mx1*-Cre^{+} *Sf3b1*$^{K700E/+}$, and *Mx1*-Cre^{+} *Srsf2*$^{P95H/+}$ *Sf3b1*$^{K700E/+}$ cells relative to *Mx1*-Cre^{+} WT cells in any replicate. The left- and right-hand columns contain sequence logos created for the intron-proximal and intron-distal 3' splice sites. **(D)** Bar plots illustrating enrichment of different variants of the SSNG (S = C or G; N = any nucleotide) exonic splicing enhancer in *Mx1*-Cre^{+} *Srsf2*$^{P95H/+}$, *Mx1*-Cre^{+} *Sf3b1*$^{K700E/+}$, and *Mx1*-Cre^{+} *Srsf2*$^{P95H/+}$ *Sf3b1*$^{K700E/+}$ cells relative to *Mx1*-Cre^{+} WT cells. Enrichment computed using the alternatively spliced sequence for cassette exons that are differentially spliced in the indicated genotype comparisons. **(E)** Scatter plots of constitutive intron splicing in *Mx1*-Cre^{+} *Srsf2*$^{P95H/+}$, *Mx1*-Cre^{+} *Sf3b1*$^{K700E/+}$, and *Mx1*-Cre^{+} *Srsf2*$^{P95H/+}$ *Sf3b1*$^{K700E/+}$ cells relative to *Mx1*-Cre^{+} WT cells for replicate B. Axes indicate the fraction of mRNAs for which each constitutive intron is removed. Red and blue indicate constitutive introns that are preferentially spliced or retained, respectively, in mutant relative to wild-type cells. **(F)** Venn diagram showing the overlap between splicing events that were significantly dysregulated in *Mx1*-Cre^{+} *Srsf2*$^{P95H/+}$, *Mx1*-Cre^{+} *Sf3b1*$^{K700E/+}$, and *Mx1*-Cre^{+} *Srsf2*$^{P95H/+}$ *Sf3b1*$^{K700E/+}$ cells relative to *Mx1*-Cre^{+} WT cells for replicate B. Example genes illustrated below are indicated with arrows. **(G)** Gene Ontology (GO) enrichment analysis of *Vav*-Cre^{+} *Srsf2*$^{P95H/+}$, *Vav*-Cre^{+} *Sf3b1*$^{K700E/+}$, and *Vav*-Cre^{+} *Srsf2*$^{P95H/+}$ *Sf3b1*$^{K700E/+}$ cells relative to *Vav*-Cre^{+} WT cells. Circle size indicates the magnitude of the p value for each term and genotype comparison. **(H)** Scatter plots of retained introns (top), competing 3' splice sites (middle), and cassette exon inclusion (bottom) in *Vav*-Cre^{+} *Srsf2*$^{P95H/+}$, *Vav*-Cre^{+} *Sf3b1*$^{K700E/+}$, and *Vav*-Cre^{+} *Srsf2*$^{P95H/+}$ *Sf3b1*$^{K700E/+}$ cells relative to *Vav*-Cre^{+} WT cells. Axes indicate the fraction of mRNAs containing each cassette exon in the indicated sample. Red and blue indicate cassette exons whose inclusion is promoted or repressed, respectively, in mutant relative to wild-type cells. **(I)** Venn diagram

showing the overlap between splicing events that were significantly dysregulated in *Vav*-Cre^{+} *Srsf2*$^{P95H/+}$, *Vav*-Cre^{+} *Sf3b1*$^{K700E/+}$, and *Vav*-Cre^{+} *Srsf2*$^{P95H/+}$ *Sf3b1*$^{K700E/+}$ cells relative to *Vav*-Cre^{+} WT cells.

Figure S5

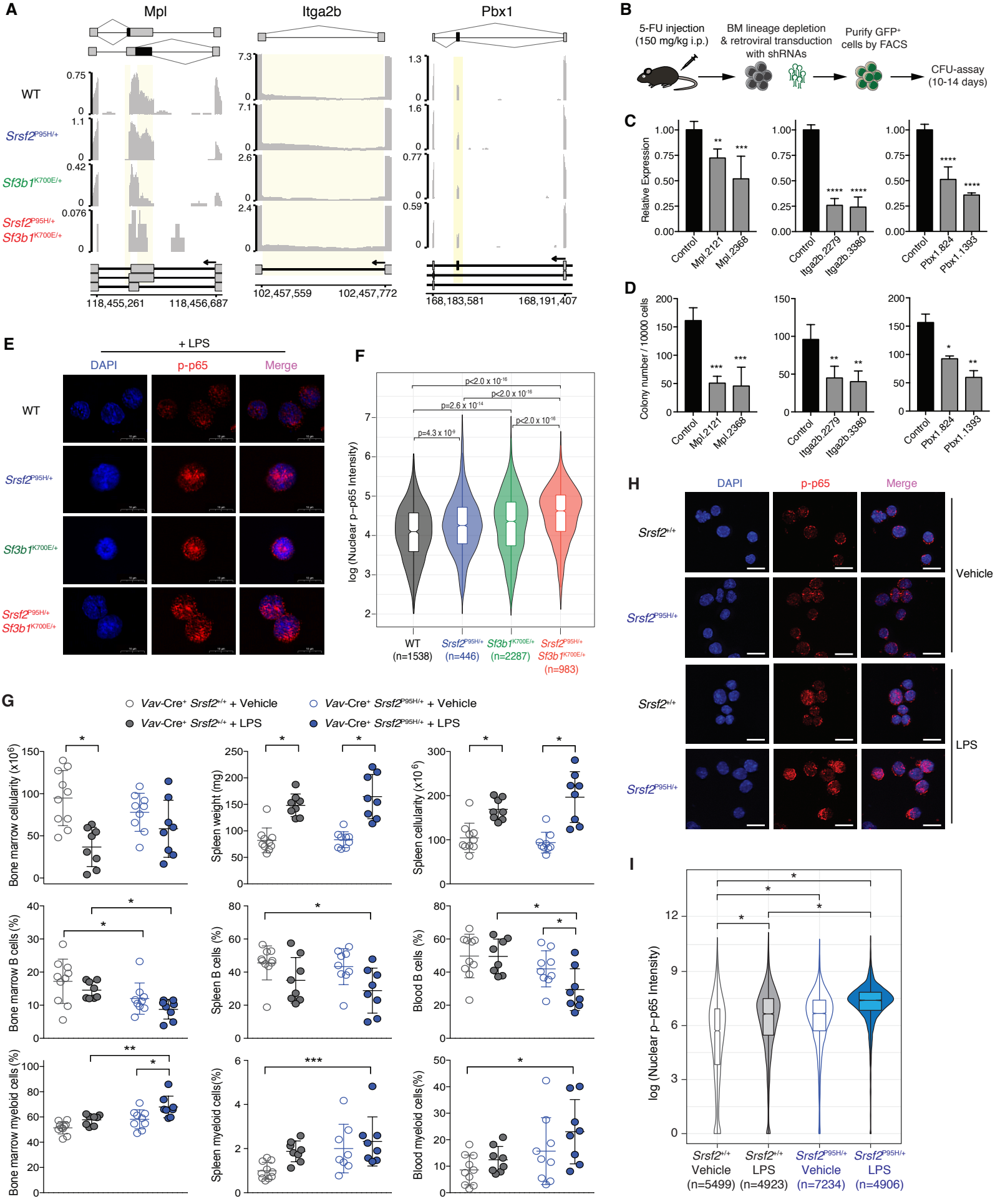
A
Mpl
Itga2b
Pbx1
WT
Srsf2P95H/+
Sf3b1K700E/+
Srsf2P95H/+ Sf3b1K700E/+
118,455,261
118,456,687
102,457,559
102,457,772
168,183,581
168,191,407
B
5-FU injection (150 mg/kg i.p.)
BM lineage depletion & retroviral transduction with shRNAs
Purify GFP+ cells by FACS
CFU-assay (10-14 days)
C
Relative Expression
Control
Mpl.2121
Mpl.2368
Itga2b.2279
Itga2b.3380
Pbx1.824
Pbx1.1393
D
Colony number / 10000 cells
E
+ LPS
DAPI
p-p65
Merge
F
log (Nuclear p−p65 Intensity)
p<2.0 x 10-16
p=2.6 x 10-14
p=4.3 x 10-9
WT (n=1538)
Srsf2P95H/+ (n=446)
Sf3b1K700E/+ (n=2287)
Srsf2P95H/+ Sf3b1K700E/+ (n=983)
G
Vav-Cre+ Srsf2+/+ + Vehicle
Vav-Cre+ Srsf2+/+ + LPS
Vav-Cre+ Srsf2P95H/+ + Vehicle
Vav-Cre+ Srsf2P95H/+ + LPS
Bone marrow cellularity (x10^6)
Spleen weight (mg)
Spleen cellularity (x10^6)
Bone marrow B cells (%)
Spleen B cells (%)
Blood B cells (%)
Bone marrow myeloid cells (%)
Spleen myeloid cells(%)
Blood myeloid cells(%)
H
DAPI
p-p65
Merge
Srsf2+/+
Srsf2P95H/+
Vehicle
LPS
I
log (Nuclear p−p65 Intensity)
Srsf2+/+ Vehicle (n=5499)
Srsf2+/+ LPS (n=4923)
Srsf2P95H/+ Vehicle (n=7234)
Srsf2P95H/+ LPS (n=4906)

Figure S5 (Related to Figure 5). Co-expression of *Srsf2* and *Sf3b1* mutations results in aberrant splicing and expression of regulators of hematopoietic stem cell survival and quiescence, as well as increased sensitivity to LPS-induced NF-κB signaling. (A) RNA-seq read coverage across the genomic loci containing the illustrated differentially spliced events in Mpl, Itga2b and Pbx1 for all genotypes. Yellow indicates the differentially spliced sequence for each event. **(B)** Schema of evaluation of the effects of shRNA mediated knockdown of Mpl, Itga2b and Pbx1 on 5-fluorouracil-treated, lineage-depleted bone marrow (BM) cells from 8-12 week-old C57BL/6 WT mice. **(C)** Quantitative RT-PCR (qRT-PCR) for Mpl, Itga2b or Pbx1 in lineage-negative (Lin^-) bone marrow cells treated with the indicated shRNAs or control shRNA. **(D)** Colony numbers from Lin^- HSPCs following shRNA-mediated knockodown of Mpl, Itga2b and Pbx1 cells. Error bars represent mean±standard deviation. Analysis of variance followed by Tukey's post-hoc test was used to compare differences between groups. **p<0.01 and ****p<0.0001. **(E)** Immunofluorescence analysis of nuclear phosphorylated-p65 (p-p65) in LK cells from *Vav*-Cre^+ WT, *Vav*-Cre^+ *Srsf2*$^{P95H/+}$, *Vav*-Cre^+ *Sf3b1*$^{K700E/+}$, and *Vav*-Cre^+ *Srsf2*$^{P95H/+}$ *Sf3b1*$^{K700E/+}$ mice following stimulation with lipopolysaccharide (LPS; 200 ng/mL; 15 min) *ex vivo*. Scale bar: 10 μm. **(F)** Violin plots showing quantitation of nuclear p-p65 intensity of LK cells following LPS stimulation from (I). Analysis of variance using Kruskal-Wallis ranked test was performed. Multiple pair-wise comparisons were adjusted by false-discovery rate (FDR). **(G)** Phenotypic analysis of bone marrow, spleen, and blood from *Vav*-Cre^+ *Srsf2*$^{+/+}$ and *Vav*-Cre^+ *Srsf2*$^{P95H/+}$ mice following chronic lipopolysaccharide (LPS) or vehicle exposure. Error bars represent mean±standard deviation. Analysis of variance followed by Tukey's post-hoc test was used to compare differences between groups, and each p value shown has been adjusted to account for multiple comparisons. *p<0.05 , **p<0.01, and ***p<0.001. **(H)** Immunofluorescence of phosphorylated p65 (p-p65) intensity from FACS-purified LSK cells following acute exposure to LPS (200 ng/mL; 15 min) *ex vivo*. Scale bar: 10 μm. **(I)** Violin plots showing quantitation of p-p65 intensity in the nucleus of LSK cells following LPS stimulation of the following groups: *Vav*-Cre^+ *Srsf2*$^{+/+}$ treated with vehicle (n=5499), *Vav*-Cre^+ *Srsf2*$^{+/+}$ treated with LPS (n=4923), *Vav*-Cre^+ *Srsf2*$^{P95H/+}$ treated with vehicle (n=7234), and *Vav*-Cre^+ *Srsf2*$^{P95H/+}$ treated with LPS (n=4906). Analysis of variance using Kruskal-Wallis ranked test was performed. Multiple pair-wise comparisons were adjusted by false-discovery rate. *p<$2.2x10^{-16}$.

Figure S6

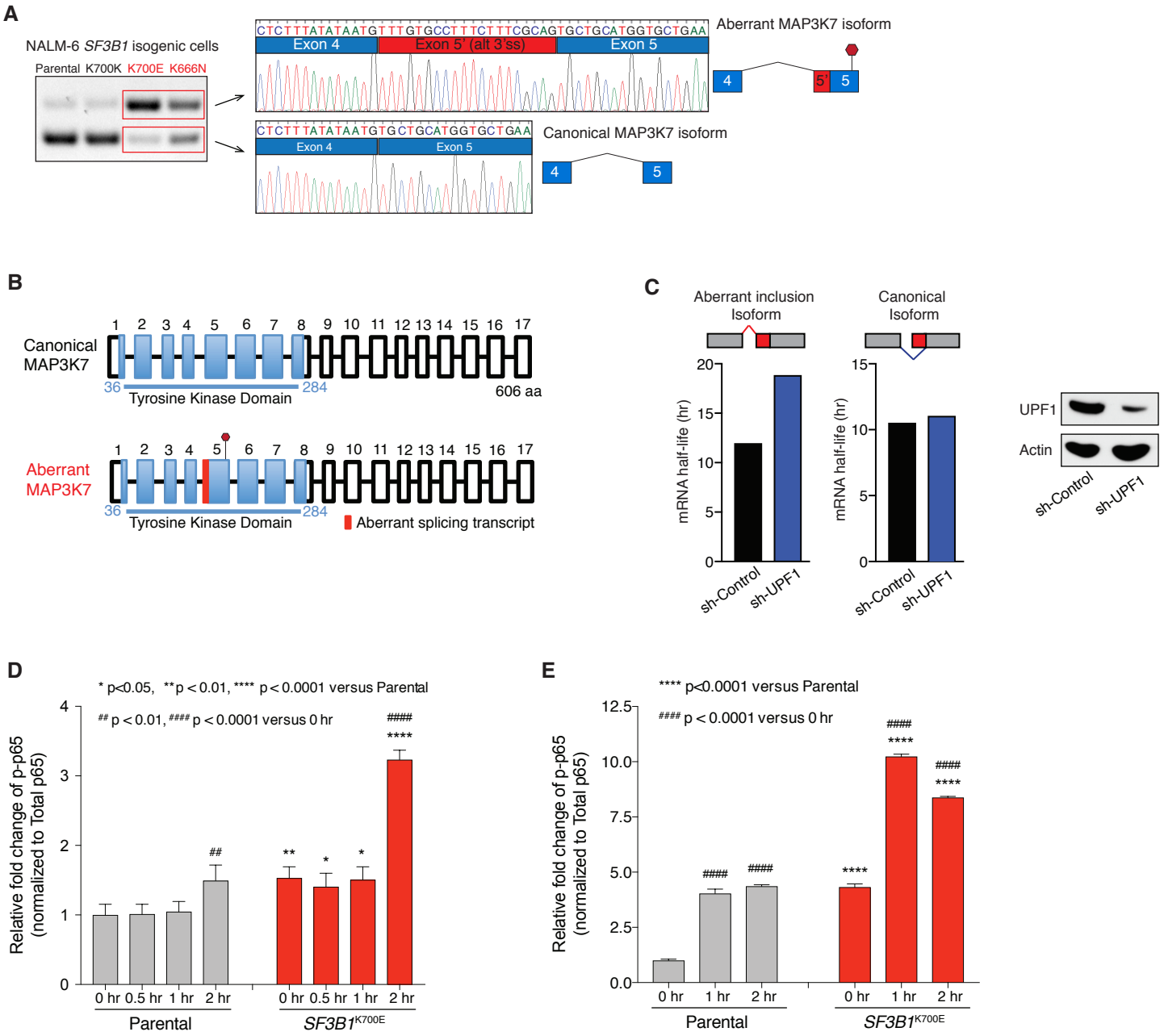
A
NALM-6 SF3B1 isogenic cells
Parental K700K K700E K666N
CTCTTTATATAATGTTTGTGCCTTTCTTTCGCAGTGCTGCATGGTGCTGAA
Exon 4
Exon 5' (alt 3'ss)
Exon 5
Aberrant MAP3K7 isoform
4
5'
5
CTCTTTATATAATGTGCTGCATGGTGCTGAA
Exon 4
Exon 5
Canonical MAP3K7 isoform
4
5
B
Canonical MAP3K7
1 2 3 4 5 6 7 8 9 10 11 12 13 14 15 16 17
36
284
Tyrosine Kinase Domain
606 aa
Aberrant MAP3K7
1 2 3 4 5 6 7 8 9 10 11 12 13 14 15 16 17
36
284
Tyrosine Kinase Domain
Aberrant splicing transcript
C
Aberrant inclusion Isoform
Canonical Isoform
mRNA half-life (hr)
20
15
10
5
0
sh-Control
sh-UPF1
mRNA half-life (hr)
15
10
5
0
sh-Control
sh-UPF1
UPF1
Actin
sh-Control
sh-UPF1
D
* p<0.05, ** p < 0.01, **** p < 0.0001 versus Parental
p < 0.01, #### p < 0.0001 versus 0 hr
Relative fold change of p-p65 (normalized to Total p65)
4
3
2
1
0
##
**
*
*
####
****
0 hr 0.5 hr 1 hr 2 hr
Parental
0 hr 0.5 hr 1 hr 2 hr
SF3B1K700E
E
**** p<0.0001 versus Parental
p < 0.0001 versus 0 hr
Relative fold change of p-p65 (normalized to Total p65)
12.5
10.0
7.5
5.0
2.5
0.0
####
####
####
****
****
****
0 hr 1 hr 2 hr
Parental
0 hr 1 hr 2 hr
SF3B1K700E

Figure S6 (Related to Figure 6). *SF3B1* mutations promote mis-splicing of MAP3K7, resulting in hyperactivation of NF-κB signaling. (A) RT-PCR analysis and Sanger sequencing traces of the normal and aberrantly spliced MAP3K7 isoforms in NALM-6 *SF3B1* isogenic cells. **(B)** Protein diagram of MAP3K7 indicating region of aberrant 3' splice site usage in *SF3B1*-mutant cells. **(C)** mRNA half-life measurements of MAP3K7 3' splice site inclusion (left) and exclusion (right) isoforms in *SF3B1*^{K700E} K562 cells. UPF1 knockdown efficiency in these cells is shown by immonoblot. **(D)** Quantitation of immunoblot densitometry of Figure 6E. **(E)** Quantitation of immunoblot densitometry of Figure 6F. Analysis of variance followed by Tukey's post-hoc test was used to compare groups.

Figure S7

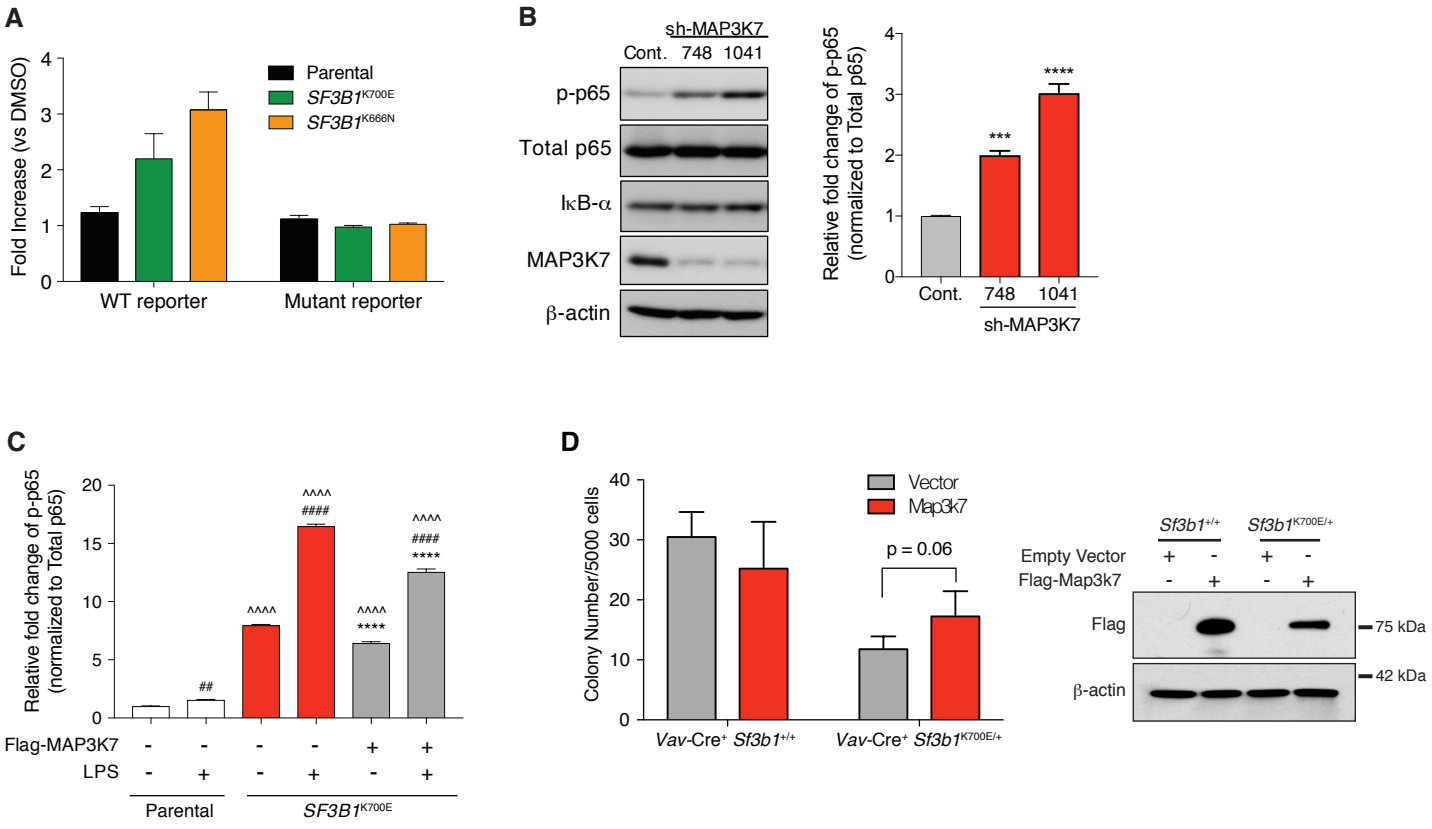
A
Fold Increase (vs DMSO)
Parental
SF3B1K700E
SF3B1K666N
WT reporter
Mutant reporter
B
sh-MAP3K7
Cont. 748 1041
p-p65
Total p65
IκB-α
MAP3K7
β-actin
Relative fold change of p-p65 (normalized to Total p65)
Cont. 748 1041
sh-MAP3K7
C
Relative fold change of p-p65 (normalized to Total p65)
Flag-MAP3K7
LPS
Parental
SF3B1K700E
D
Colony Number/5000 cells
Vector
Map3k7
p = 0.06
Vav-Cre+ Sf3b1+/+
Vav-Cre+ Sf3b1K700E/+
Sf3b1+/+
Sf3b1K700E/+
Empty Vector
Flag-Map3k7
Flag
β-actin
75 kDa
42 kDa

Figure S7 (Related to Figure 7). MAP3K7 loss results in hyperactive NF-κB signaling in *SF3B1*-mutant cells. (A) Fold-change in luciferase activity of NALM-6 isogenic cells transfected with a wildtype NF-κB luciferase reporter or a version of the reporter where all five NF-κB response elements were mutagenized. **(B)** Immunoblot of p-p65, IκB-α, MAP3K7, and loading controls in K562 cells treated with anti-MAP3K7 shRNAs. Quantitation of immunoblot densitometry (left). **(C)** Quantitation of immunoblot densitometry of Figure 7D. Error bars represent mean±standard deviation. Analysis of variance followed by Tukey's post-hoc test was used to compare groups. ***p<0.001 versus sh-Control or parental, ****p<0.0001 versus parental, ## p<0.01 versus unstimulated, ### p<0.001 versus unstimulated, ^^^^p<0.0001 parental. **(D)** Numbers of hematopoietic colonies 10-14 days after Map3k7 cDNA expression in lineage-negative (Lin^-) cells from *Vav*-Cre^+ *Sf3b1*$^{K700E/+}$ and *Vav*-Cre^+ WT E14.5 fetal liver cells (Left). Immunoblot analysis of Flag-tagged Map3k7 cDNA from hematopoietic colonies derived from *Vav*-Cre^+ *Sf3b1*$^{+/+}$ and *Vav*-Cre^+ *Sf3b1*$^{K700E/+}$ cells (Right).

Figure S8

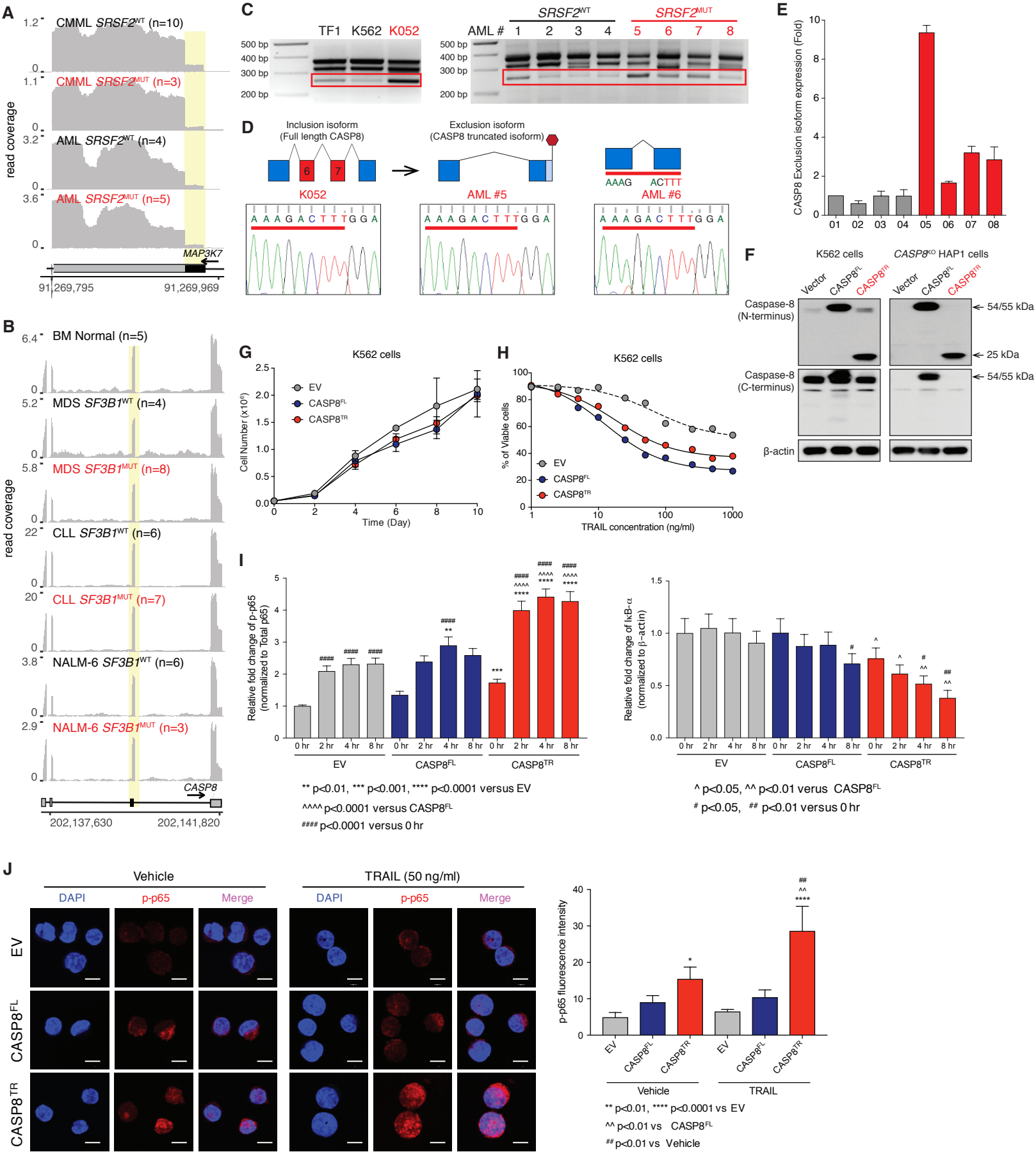
A
CMML SRSF2WT (n=10)
CMML SRSF2MUT (n=3)
AML SRSF2WT (n=4)
AML SRSF2MUT (n=5)
read coverage
MAP3K7
91,269,795
91,269,969
B
BM Normal (n=5)
MDS SF3B1WT (n=4)
MDS SF3B1MUT (n=8)
CLL SF3B1WT (n=6)
CLL SF3B1MUT (n=7)
NALM-6 SF3B1WT (n=6)
NALM-6 SF3B1MUT (n=3)
read coverage
CASP8
202,137,630
202,141,820
C
TF1 K562 K052
500 bp
400 bp
300 bp
200 bp
SRSF2WT
SRSF2MUT
AML # 1 2 3 4 5 6 7 8
D
Inclusion isoform
(Full length CASP8)
Exclusion isoform
(CASP8 truncated isoform)
6
7
AAAG ACTTT
K052
AML #5
AML #6
A A A G A C T T T G G A
E
CASP8 Exclusion isoform expression (Fold)
01 02 03 04 05 06 07 08
F
K562 cells
CASP8KO HAP1 cells
Vector
CASP8FL
CASP8TR
Caspase-8
(N-terminus)
Caspase-8
(C-terminus)
β-actin
54/55 kDa
25 kDa
G
K562 cells
EV
CASP8FL
CASP8TR
Cell Number (x10⁶)
Time (Day)
H
K562 cells
% of Viable cells
TRAIL concentration (ng/ml)
I
Relative fold change of p-p65
(normalized to Total p65)
0 hr 2 hr 4 hr 8 hr
EV
CASP8FL
CASP8TR
** p<0.01, *** p<0.001, **** p<0.0001 versus EV
^^^^ p<0.0001 versus CASP8FL
p<0.0001 versus 0 hr
Relative fold change of IκB-α
(normalized to β-actin)
^ p<0.05, ^^ p<0.01 verus CASP8FL
# p<0.05, ## p<0.01 versus 0 hr
J
Vehicle
TRAIL (50 ng/ml)
DAPI
p-p65
Merge
EV
CASP8FL
CASP8TR
p-p65 fluorescence intensity
Vehicle
TRAIL
** p<0.01, **** p<0.0001 vs EV
^^ p<0.01 vs CASP8FL
p<0.01 vs Vehicle

Figure S8

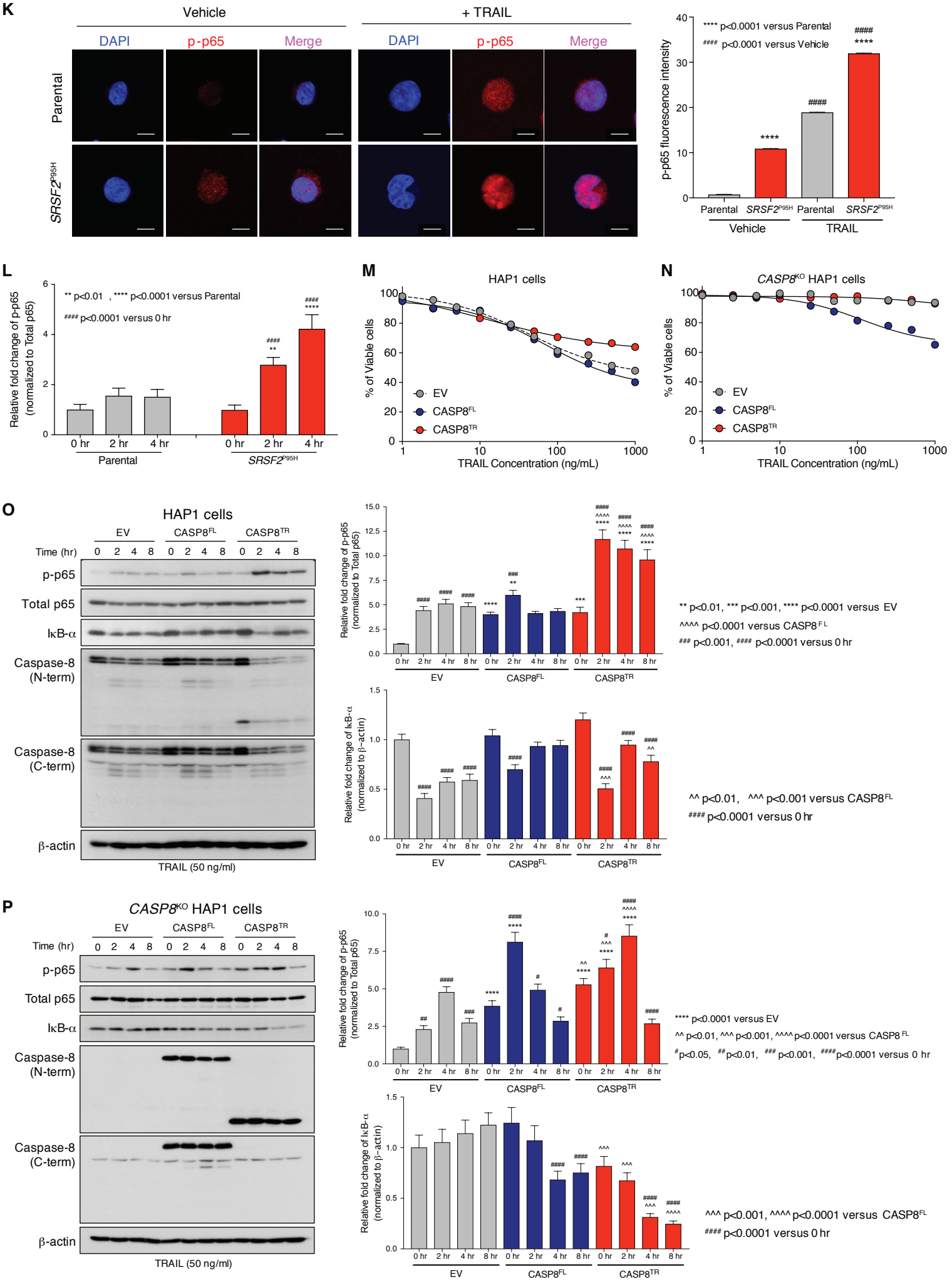
K
Vehicle
+ TRAIL
DAPI
p-p65
Merge
Parental
SRSF2P95H
p-p65 fluorescence intensity
**** p<0.0001 versus Parental
p<0.0001 versus Vehicle
Parental
SRSF2P95H
Vehicle
TRAIL
L
** p<0.01 , **** p<0.0001 versus Parental
p<0.0001 versus 0 hr
Relative fold change of p-p65 (normalized to Total p65)
0 hr
2 hr
4 hr
M
HAP1 cells
% of Viable cells
EV
CASP8FL
CASP8TR
TRAIL Concentration (ng/mL)
N
CASP8KO HAP1 cells
O
HAP1 cells
Time (hr)
p-p65
Total p65
IκB-α
Caspase-8 (N-term)
Caspase-8 (C-term)
β-actin
TRAIL (50 ng/ml)
Relative fold change of IκB-α (normalized to β-actin)
** p<0.01, *** p<0.001, **** p<0.0001 versus EV
^^^^ p<0.0001 versus CASP8FL
p<0.001, #### p<0.0001 versus 0 hr
^^ p<0.01, ^^^ p<0.001 versus CASP8FL
p<0.0001 versus 0 hr
P
CASP8KO HAP1 cells
**** p<0.0001 versus EV
^^ p<0.01, ^^^ p<0.001, ^^^^ p<0.0001 versus CASP8FL
#p<0.05, ##p<0.01, ###p<0.001, ####p<0.0001 versus 0 hr
^^^ p<0.001, ^^^^ p<0.0001 versus CASP8FL
p<0.0001 versus 0 hr

Figure S8 (Related to Figure 8). *SRSF2* mutations promote aberrant splicing of caspase-8 (CASP8) resulting in expression of a stable truncated protein that hyperactivates NF-κB signaling. (A) RNA-seq coverage plots of *MAP3K7* in acute myeloid leukemia (AML) and chronic myelomonocytic leukemia (CMML) patient samples wild-type (WT) or mutant (MUT) for *SRSF2*. **(B)** RNA-seq coverage plots of *CASP8* in normal human bone marrow (BM) cells as well as the NALM-6 cell line and cells from myelodysplastic syndrome (MDS) and chronic lymphocytic leukemia (CLL) patients wild-type (WT) or mutant (MUT) for *SF3B1.* **(C)** RT-PCR of the CASP8 splicing event in human leukemia cell lines and primary human AML patient samples WT or mutant for *SRSF2* with diagram of predicted effects of CASP8 mRNA. The red box highlights the *CASP8* isoform promoted by mutant SRSF2. **(D)** Sanger sequencing traces of the aberrant CASP8 isoform ($CASP8^{TR}$) in *SRSF2*-mutant leukemia cell line (K052) and *SRSF2*-mutant primary AML patient samples. **(E)** Quantitative RT-PCR (qRT-PCR) analysis of the aberrant CASP8 isoform expression in AML patient samples WT or mutant for *SRSF2*. **(F)** Immunoblot analysis of caspase-8 in K562 cells (left panel) and $CASP8^{KO}$ HAP1 cells (right panel) expressing cDNA constructs encoding empty vector (EV), full-length CASP8 ($CASP8^{FL}$), or the aberrantly spliced caspase-8 truncated isoform ($CASP8^{TR}$). **(G)** Growth assay of K562 cells overexpressing empty vector control (EV), full-length caspase-8 ($CASP8^{FL}$) and the aberrant caspase-8 truncated isoform ($CASP8^{TR}$). **(H)** Cell viability assay using CellTiter-Glo in K562 cells expressing empty vector control (EV), $CASP8^{FL}$, and $CASP8^{TR}$ isoforms 48 hr post-TRAIL stimulation. **(I)** Quantitation of immunoblot densitometry of Figure 8E. **(J)** Immunofluorescence analysis of phosphorylated p65 (p-p65) in K562 cells from Figure 8E with quantitation of results shown on right. Scale bar: 10 μm. **(K)** Immunofluorescence analysis of phosphorylated p65 (p-p65) in isogenic genetically modified K562 cells with or without $SRSF2^{P95H}$ mutation expressed from the endogenous *SRSF2* locus with and without TRAIL stimulation (50 ng/mL). Scale bar: 10 μm. **(L)** Quantitation of immunoblot densitometry of Figure 8G. Cell viability assay using CellTiter-Glo in **(M)** HAP1 and **(N)** $CASP8^{KO}$ HAP1 cells expressing EV control, $CASP8^{FL}$, and $CASP8^{TR}$ isoforms 48 hr post TRAIL stimulation. Analysis of NF-κB signaling following TRAIL stimulation (50 ng/mL) in **(O)** HAP1 and **(P)** $CASP8^{KO}$ HAP1 cells expressing EV, $CASP8^{FL}$, and $CASP8^{TR}$ isoforms. Quantification of immunoblot signals using densitometry is shown on right. Analysis of variance followed by Tukey's post-hoc test was used to compare groups.